PCCP

RSC Publishing

PAPER

View Article Online
View Journal | View Issue

Cite this: *Phys. Chem. Chem. Phys.*, 2013, **15**, 16725

Supramolecular design of biocompatible nanocontainers based on amphiphilic derivatives of a natural compound isosteviol†

Dinar R. Gabdrakhmanov,[a] Mikhail A. Voronin,[a] Lucia Ya. Zakharova,*[a] Alexander I. Konovalov,[a] Ravil N. Khaybullin,[a] Irina Yu. Strobykina,[a] Vladimir E. Kataev,[a] Dzhigangir A. Faizullin,[b] Natalia E. Gogoleva,[b] Tatiana A. Konnova,[b] Vadim V. Salnikov[b] and Yuriy F. Zuev[b]

Two diterpenoid surfactants with ammonium head groups and bromide (**S1**) or tosylate (**S2**) counterions have been synthesized. Exploration of these biomimetic species made it possible to demonstrate that even minor structural changes beyond their chemical nature may dramatically affect their solution behavior. While their aggregation thresholds differ inconsiderably, morphological behavior and affinity to lipid bilayer are strongly dependent on the counterion nature. Compound **S2** demonstrates properties of typical surfactants and forms small micelle-like aggregates above critical micelle concentration. For surfactant **S1**, two critical concentrations and two types of aggregates occur. Structural transitions have been observed between small micelles and aggregates with higher aggregation numbers and hydrodynamic diameter of *ca.* 150 nm. Unlike **S2**, surfactant **S1** is shown to integrate with liposomes based on dipalmitoylphosphatidylcholine, resulting in a decrease of the temperature of the main phase transition. Both surfactants demonstrate an effective complexation capacity toward oligonucleotide (ONu), which is supported by recharging the surfactant–ONu complexes and the ethidium bromide exclusion at a low N/P ratio. Meanwhile, a very weak complexation of plasmid DNA with the surfactants has been revealed in the gel electrophoresis experiment. The DNA transfer to bacterial cells mediated by the surfactant **S1** is shown to depend on the protocol used. In the case of the electroporation, the inhibition of the cell transformation occurs in the presence of the surfactant, while upon the chemical treatment no surfactant effect has been observed. The variability in the morphology, the biocompatibility, the nanoscale dimension and the high binding capacity toward the DNA decamer make it possible to nominate the designed surfactants as promising carriers for biosubstrates or as a helper surfactant for the mixed liposome–surfactant nanocontainers.

Received 9th April 2013,
Accepted 5th August 2013

DOI: 10.1039/c3cp51511g

www.rsc.org/pccp

Introduction

Amphiphilic compounds are widely used in modern strategies.[1,2] In biomedical applications, special attention is paid to the targeted delivery of drugs with poor water solubility.[3,4] Therefore, in recent years, formulations based on lipids or synthetic surfactants have attracted considerable attention as drug carriers.[5,6] Advantages and practical use of liposomes, micelles, and microemulsions are due to the presence of significant hydrophobic domains in their structure which may be used for compartmentalization of a variety of low-soluble therapeutic and diagnostic agents. In addition, these soft particles fabricated through noncovalent techniques are within the nanoscale, which is important in biomedical applications. Cationic surfactants are known to be widely explored as condensing agents in gene delivery protocols.[7,8] Meanwhile only a few of them correspond to the criterion of the biorelevancy, *i.e.*, (i) the biocompatibility of amphiphilic building blocks, which brings to a focus compounds of natural origin or bearing biofragments; (ii) the cleavability, which assumes the presence of the ester or amide groups subjected to the hydrolysis in the processes of metabolism; (iii) the occurrence of linker groups that connect the positively charged moieties with hydrophobic domains, thus distancing them from each other; (iv) the capacity of forming associates within the nanoscale dimension, which is required for a long circulation in living systems. Herein, two surfactants, the ammonium derivatives of natural diterpenoid isosteviol (16-oxo-*ent*-beyeran-19-oic acid) (Scheme S1, ESI†)[9]

[a] *A.E. Arbuzov Institute of Organic and Physical Chemistry of Kazan Scientific Center of Russian Academy of Sciences, 8 ul. Arbuzov, 420088 Kazan, Russian Federation. E-mail: lucia@iopc.ru*
[b] *Kazan Institute of Biochemistry and Biophysics of Kazan Scientific Center of the Russian Academy of Sciences, P.O.B. 30, 420111 Kazan, Russian Federation*

† Electronic supplementary information (ESI) available. See DOI: 10.1039/c3cp51511g

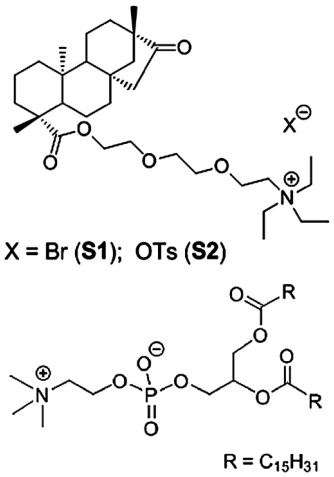

Fig. 1 Chemical structures of surfactants **S1**, **S2** and dipalmitoylphosphatidylcholine (DPPC).

are proposed as a response to these requirements. Isosteviol is one of the most important natural building blocks for the design of bioactive compounds because it exhibits a wide spectrum of biological and pharmacological activities.[10] To improve the hydrophilic characteristics, isosteviol derivatives with the alkylammonium fragment bridged by polyoxyetylene spacer (Fig. 1, Scheme S1, ESI†) are synthesized.

It is of importance that surfactants are biomimetic species that make it possible to model the basic principles of self-organization and functioning of living systems.[11–13] One of the key features of biological substances, especially amphiphiles, is that even a small variation in their structure or microenvironment conditions (pH, concentration, temperature) may be followed by a marked change in the biological events. This feature is probably one of the factors responsible for the high degree of concurrency and selectivity of bioprocesses. Therefore, we focus on the comparison of the structural behavior and functionality of two cationic surfactants of the same structure differing only in their counterions, *i.e.* surfactant **S1** with an inorganic bromide anion and surfactant **S2** with an organic tosylate anion (Fig. 1). The following points are addressed: (i) the elucidation of their structural characteristics, *i.e.* critical micelle concentration (cmc) and micellar size; (ii) the complexation of the surfactants with a decamer of nucleic acid; (iii) the transfer of DNA into cells mediated by surfactants **S1** and **S2**; (iv) their interaction with a lipid bilayer. Specifically, the interaction of the surfactants with liposomes based on dipalmitoylphosphatidylcholine (DPPC) (Fig. 1) is studied.

Experimental

Materials

Dipalmitoylphosphatidylcholine (Sigma), ethidium bromide (EB) (Sigma-Aldrich), cetylpyridinium bromide (CPB) (AppliChem, BioChemica, Germany) and pyrene for fluorescence ($\geq$99%) (Sigma) were used as received. The oligonucleotide (ONu) of 10 base pairs, strand 2 (GCGTTAACGC, molecular weight 3028) was purchased from Joint Stock Company Syntol (Moscow, Russia). Stock solution of ONu was initially prepared in the tris-HCl buffer (4 mM; pH 8.0), then diluted to 10 mM, heated at 95 °C for 5 min and immediately chilled in an ice bath.

Synthesis

All reagents used were of analytical grade. Solvents were dried if necessary by standard methods. Column chromatography was performed on silica gel (particle size 63–200 mm) using light petroleum–EtOAc as an eluent. Isosteviol was prepared by acid hydrolysis of sweetener Sweta (enzymatically treated glycosides of the plant *S. rebaudiana* manufactured by Stevian Biotechnology Corporation, Kuala Lumpur, Malaysia) as previously described.[14] Additional details are given in the ESI.†

Turbidimetry

The phase transitions of surfactant–DPPC mixtures were studied using a Lambda 25 (Perkin Elmer) double-beam spectrophotometer, equipped with a Peltier-controlled thermostated cell holder, using quartz cells of 1 cm pathlength. Before turbidity measurements the samples were diluted to the 0.7 mM DPPC concentration in a buffer. The reference cell was filled with buffer alone. The sample cells were capped to prevent evaporation. Turbidity was measured at 350 nm, and turbidity values were recorded as a function of temperature with the sample continuously stirred during heating. The heating rate was 0.1 °C min^{-1}, with temperature varied between 35 and 45 °C. Small volumes of concentrated surfactant were added to the same sample, and temperature scans were repeated. Turbidity traces were approximated by the van't Hoff two-state model equation yielding half-transition temperature values. Sample preparation is given in the ESI.†

Dynamic light scattering

Dynamic light scattering (DLS) measurements were performed by means of Malvern Instrument Zetasizer Nano. The measured autocorrelation functions were analyzed by the Malvern DTS software and the second-order cumulant expansion methods. The effective hydrodynamic radius (R_H) was calculated according to the Stokes–Einstein relation: $D_S = k_B T/6\pi\eta R_H$, in which D_S is the diffusion coefficient, k_B is the Boltzmann constant, T is the absolute temperature, and η is the solvent viscosity. For zeta potential measurements, Zeta potential Nano-ZS (MALVERN) using laser Doppler velocimetry and phase analysis of light scattering was used. The temperature of the scattering cell was controlled at 25 °C; the data were analyzed with the software supplied for the instrument. DLS and zeta potential titration measurements had no less than ten measurements in ten runs, so that $\geq$100 scans for each surfactant/ONu ratio were obtained. Only multiple reproducible results were taken into account, thereby they differed by less than 3%.

Transmission electron microscopy (TEM)

The prepared surfactant suspensions were processed by using copper grids to adsorb aggregated particles from the suspension, then stained in 2.5% uranyl acetate for 30 seconds and dried.[15,16]

The specimen was observed under a JEM 1200EX transmission electron microscope (JEOL, Japan) operated at 80 kV.

Ethidium bromide (EB) exclusion studies

Fluorescence spectra of ONu–EB complexes were recorded from 500 to 700 nm, with a spectrofluorometer Fluorat-02-Panorama (Lumex, Russia) with a precise thermostat (Huber CC1, Germany). Sample preparation is given in the ESI.†

Solubilization of Sudan I and pyrene

1-Phenylazonaphth-2-ol (Sudan I) and pyrene (Py) were used as received. The solubilization experiments were performed by adding an excess of crystalline probe either to single surfactant solutions or to the surfactant–DPPC mixture. These solutions were allowed to equilibrate for about 48 h at room temperature. They were filtered, and their absorbance was measured at 500 nm (Sudan) or 309 nm (Py) using the Specord-250 Plus spectrophotometer. Extinction coefficients of probes were equal to 7800 and 47 680 M^{-1} cm^{-1} for Sudan I and Py respectively. Quartz cuvettes containing the sample were used, with a width of 0.2 or 0.5 cm, and the absorbency measured was reduced to the 1 cm pathlength.

Fluorescence spectroscopy

The fluorescence spectra of pyrene (1×10^{-6} mol L^{-1}) in **S1** and **S2** solutions in the absence of (Fig. S1, ESI†) and in the presence of (Fig. S2, ESI†) a quencher (cetylpyridinium bromide) were recorded at 25 °C in a Varian Cary Eclipse spectrofluorimeter. Sample excitation was at a wavelength of 335 nm. Emission spectra were recorded in 350–500 nm. The thickness of the cell was 10×10 mm. The scanning speed was 120 nm min^{-1}. Fluorescence intensities of the first peak at 373 nm (I_I), of the third peak at 384 nm (I_{III}), and of the peak at 394 nm were obtained from the spectra. The determination of aggregation numbers was performed by the most intense peak at 394 nm. The N values were calculated from the dependence (eqn (1)):[17]

$$\ln(I_0/I) = [N/(C - \text{cmc})]\,[Q], \quad (1)$$

where I_0 and I are the intensities of the fluorescence of pyrene in the absence and presence of a quencher, respectively; C is the total surfactant concentration; $[Q]$ is the concentration of the quencher. The cmc value was determined from the dependence of the intensity ratio of the first and third peaks on the surfactant concentration.[18]

Gel retardation assay

The electrophoretic mobility of the surfactant–DNA complexes was determined by gel electrophoresis using 1.0% agarose gel in 40 mM tris-acetate buffer with 1 mM EDTA at pH 8.0. Experiments were run at a constant voltage of 80 V. About 800 ng of plasmid pK18 in 25 μL of solution was mixed with different amounts of surfactant solutions to achieve the desired charge ratio and then incubated for 2 h prior to running the gel. DNA was visualized under the UV illumination by staining the gels with ethidium bromide at room temperature.

Transformation procedure

E. coli Nova Blue cells were grown in LB (Luria-Bertani) broth to the early exponential phase up to the optical density OD_{600} 0.4–0.5. Preparation of competent cells and electroporation were performed by the standard method.[19] The preparation of competent cells and $CaCl_2$/heat shock transformation were performed according to ref. 20. Competent cells were stored at −70 °C until needed. Frozen cells were thawed on ice and used immediately in the transformation assay. To determine the efficiency of transformation in the presence of various concentrations of surfactant **S1** 10 ng of pK18 plasmid DNA was incubated with different concentrations of surfactant (the ratio of nitrogen/phosphorus, N/P, equaled 0.001, 0.1, 2, and 10, respectively). The colony-forming units (CFU) on plate per μg of vector DNA with no **S1** were used as control and taken as 100%. The uncertainty in the obtained data was determined using the Student's t-test. The data corresponding to criterion $P < 0.05$ were considered statistically significant. The data are presented as mean SD (standard deviation) for at least three independent experiments (Tables S1 and S2, ESI†).

Results and discussion

Aggregation of surfactants

A generally accepted method for the investigation of the aggregation of ionic surfactants is conductometry. Fig. 2 shows the conductivity data which demonstrate a critical character with breakpoints at concentrations of 12.0 and 9.7 mM for **S1** and **S2**, respectively. Unexpectedly, a low difference occurs in micellization properties of these surfactants, despite the more hydrophobic counterion of **S2**.

On the contrary, the cmc values of typical cationic surfactants, cetyl trimethylammonium bromide (CTAB) and tosylate (CTAT),[21] differ significantly. In comparison with the alkyl trimethylammonium surfactant series, cmcs of **S1** and **S2** are close to their dodecyl homolog, despite the fact that the number of carbon atoms in the hydrophobic fragments of **S1** and **S2** are higher. This probably results from the bulky geometry of the

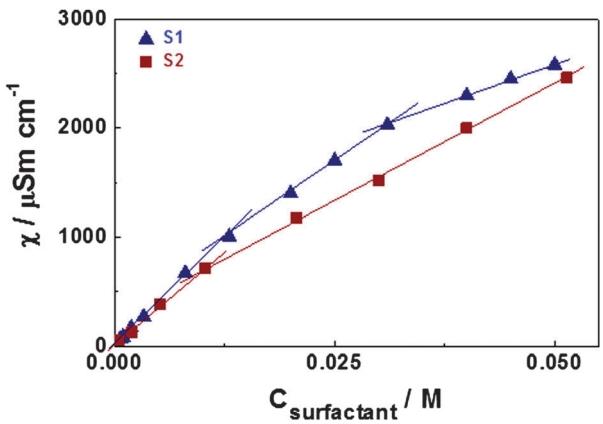

Fig. 2 Specific conductivity as function of surfactant concentration for aqueous **S1** and **S2** solutions; 25 °C.

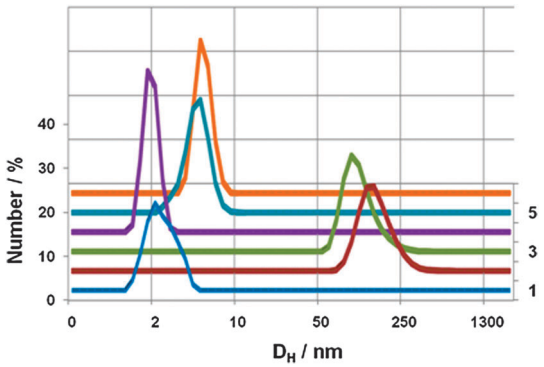

Fig. 3 The DLS data given as a number averaged size distribution for **S1** (1–4) and **S2** (5 and 6) at their different concentrations: 10 mM (1), 17.5 mM (2), 20 mM (3), 30 mM (4), 15 mM (5), 30 mM (6); tris-buffer; pH 7.0; 25 °C.

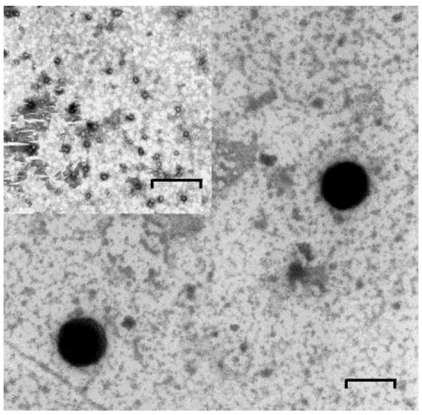

Fig. 4 Negative staining electron micrographs of aggregates formed in the 20 mM **S1** sample; bar is 200 nm (the inset shows the image for the 10 mM **S1** sample; bar is 100 nm).

diterpenoid scaffold, which prevents the close packing of molecules upon aggregation. It should be emphasized that a second breakpoint appears in the conductivity plot of **S1** around 0.025–0.03 M, which can indicate the change in the solution behavior, *e.g.* the structural re-arrangement of aggregates. To test the significance of the second breakpoint and probability of morphological transition in the case of **S1**, dynamic light scattering measurements are involved. DLS data shown in Fig. 3 reveal that the difference occurs between the size characteristics of **S1** and **S2**. Aggregates with the hydrodynamic diameter D_H from 3 to 5 nm are observed within the whole concentration range of **S2**. In the case of **S1**, small micelle-like aggregates are formed at concentrations close to the cmc, while large aggregates (D_H of *ca.* 150 nm) are revealed in the wide concentration range between the cmc and the transition point of *ca.* 0.025–0.03 M, thus confirming the validity of structural re-arrangement assumed and the essential difference in the solution behavior of surfactants. It can be assumed that aggregates of different morphologies occur in the **S1** system, namely, assemblies with the size of ≤ 5 nm are spherical micelles, while larger aggregates are probably colloid particles with a lower surface curvature and higher aggregation numbers, *e.g.* vesicles.[22] The occurrence of two types of aggregates in the **S1** solutions is also evidenced from the TEM images (Fig. 4). Small micelle-like particles exist near the cmc, while aggregates of *ca.* 150 nm appear in the 20 mM **S1** sample.

To characterize the intrinsic properties of self-assembling systems, spectral probes are successively used. Among them Py is one of the most informative and widely studied.[18,23] Since it is a highly hydrophobic probe, its solubility markedly increases in surfactant solutions above the cmc due to the incorporation of the probe into the nonpolar micellar interior. This makes it possible to examine such important properties as cmc, micropolarity, aggregation number and solubilization capacity of **S1** and **S2** aggregates (Fig. 5).

The ratio of intensities of the first and third vibronic bands of fluorescence emission spectra of Py is known to be sensitive to the micropolarity of the location site of the probe.[18] The value (I_1/I_3) is the highest in water (*ca.* 1.8) and decreases with a decrease in the polarity of the microenvironment.

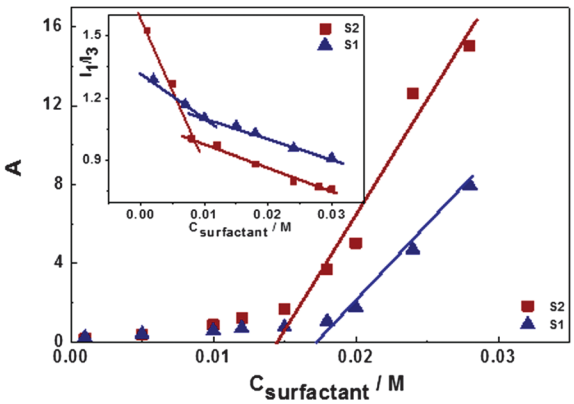

Fig. 5 The optical density of Py in **S1** and **S2** aqueous solutions *vs.* surfactant concentration; 25 °C (at inset: the ratio of the first and the third vibronic peaks of Py *vs.* surfactant concentration plot in **S1** and **S2** aqueous solutions; 25 °C).

Therefore, the I_1/I_3 *versus* surfactant concentration dependence is often used for monitoring the formation of micelles, including the determination of cmc and the characterization of micropolarity. The inset of Fig. 5 shows such plots for **S1** and **S2** solutions, demonstrating critical behavior with cmcs at about 10 mM. More marked changes of the I_1/I_3 ratio occur in the case of **S2** as compared to **S1**. This can be due either to the different packing modes or different locations of Py in the aggregates. The lower I_1/I_3 ratio for the **S2** sample above the cmc probably indicates that the deeper localization of Py in the aggregate interior occurs in the case of **S2** as compared to **S1**. Besides, the I_1/I_3 ratio depends not only on the micropolarity but also on the aggregation number and core size, therefore pyrene will be less influenced by water molecules with an increase in the size of aggregates.[24,25]

Analysis of the intensities of fluorescence of pyrene in the absence and presence of quencher (CPB) in terms of eqn (1) yields aggregation numbers of aggregates (Fig. 6; Table 1). In the case of **S2**, aggregation numbers of *ca.* 50–60 are observed within the whole concentration range studied. This is in good agreement with the formation of micelle-like aggregates.

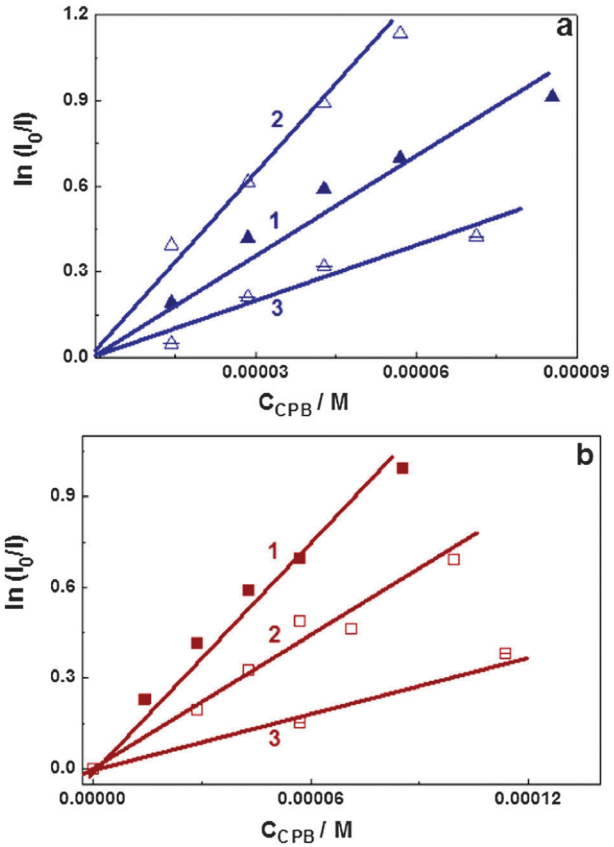

Fig. 6 Logarithm of the ratio of fluorescence intensity in the absence and presence of quencher (cetylpyridinium bromide) *vs.* quencher concentration plots for **S1** and **S2** aqueous solutions; surfactant concentrations are equal to 15 mM (1), 20 mM (2), 25 mM (3), 25 °C.

Table 1 The characteristic parameters of **S1** and **S2**: aggregation numbers (N), the first stepwise association constant (K_1), the free energy (ΔG°), and the number of pyrene molecules per micelle (R_{pm})[a]

	N (mM)					
Surfactant	15	20	25	$10^{-5}\cdot K_1$ (L mol^{-1})	ΔG° (kJ mol^{-1})	R_{pm}[b]
S1	72	164	45	16.08	−35.4	0.86
S2	59	61	49	11.44	−34.6	0.60

[a] At surfactant concentration 20 mmol L^{-1}. [b] $C_P^V = 5.3 \times 10^{-7}$ M.[26]

Another trend is observed for the **S1** solutions, in which a sharp increase of N values from 72 to 164 occurs beyond the cmc, followed by a decrease of aggregation numbers at the surfactant concentration of 25 mM. These data give evidence in support of the assumption on the micelle–vesicle–micelle transition[22] in the **S1** system.

Fig. S3 (ESI†) and Fig. 5 show UV spectroscopy data indicating an increase in the Py absorbance beyond the concentrations of 0.014 and 0.0175 M, which were attributed to the cmc values of **S1** and **S2**. They are somewhat higher as compared to those obtained from conductivity measurements probably due to the low solubilization capacity of the primary aggregates formed at the conductometry cmc. The absorbance data (Fig. S4, ESI†) make it possible to calculate the partition of Py between the micellar and volume phases, taking into account the Lambert–Beer law:

$$\frac{A_t - A_{cmc}}{A_{cmc}} = \frac{C_P^M}{C_P^V}, \quad (2)$$

where A_{cmc} and A_t are the optical density at the cmc and at arbitrary surfactant concentration beyond the cmc, and C_P^M and C_P^V are the concentrations of Py in the micelle and in water, respectively.

In terms of the stepwise association equilibria model,[26] the Py partition can be yielded as follows:

$$\frac{C_P^V}{C_P^M} = \frac{K_1}{N}(C - \text{cmc}); \quad (3)$$

here C is the surfactant concentration beyond the cmc, K_1 is the first stepwise association constant between the pyrene molecule and the vacant micelle, and N is the aggregation number of a micelle. The free energy of the pyrene incorporation into micelles (ΔG°) and the numbers of pyrene molecules per micelle (R_{pm}) can be calculated using expressions (4) and (5):

$$\Delta G^\circ = -RT \ln K_1. \quad (4)$$

$$R_{pm} = K_1 C_P^V. \quad (5)$$

Table 1 summarizes the parameters calculated *via* eqn (2)–(5). They are close to the values obtained in the Py solubilization study in cationic surfactant solutions by other authors.[27,28] The higher K_1 and R_{pm} values obtained for the **S1** system probably reflect the larger size and aggregation numbers of the **S1** aggregates.

Thus, the data collected strongly support the idea of the significant role of the counterion nature in the solution behavior of diterpenoid surfactants. On the one hand, this is important from the viewpoint of the insight into the mechanism of the functioning of biosystems and their high specificity, while on the other it may be used for the design of the soft nanomaterials for bioapplications. In the following sections, their potentiality with regard to bioapplications is considered.

The surfactant–oligonucleotide complexation

We have recently studied the complexation of cationic surfactants with oligo- and polynucleotides.[29,30] Different mechanisms are shown to contribute to the interaction including electrostatic forces and hydrophobic effect. Surfactants **S1** and **S2** can be considered as potential candidates for nonviral vectors since both cationic centers and hydrophobic fragments are available in their molecules, thus providing the affinity to the negatively charged phosphate moieties of nucleotide bases and cell lipid membranes at the same time. A wide involvement of amphiphilic cationic agents in gene delivery protocols is based on two key effects: the neutralization of charges of phosphate anions and the compactization of the giant DNA molecules upon complexation with cationic species. Therefore the zeta potential and size behavior of surfactant–ONu complexes were monitored at a different N/P ratio.

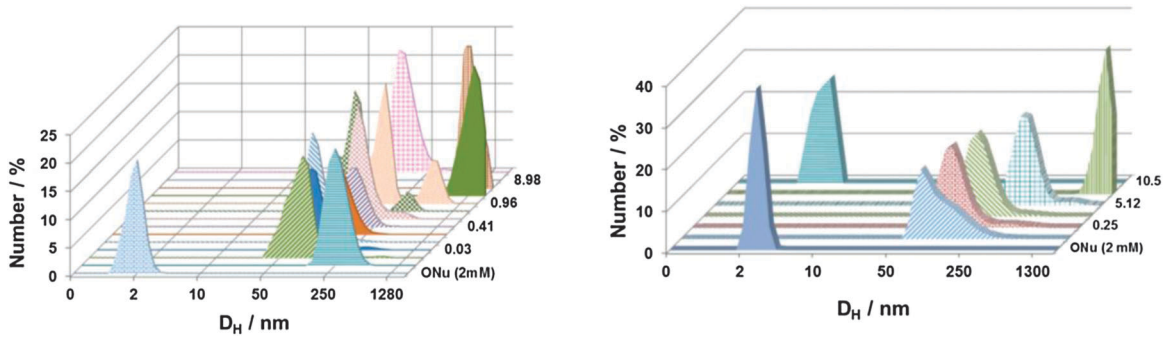

Fig. 7 Number averaged size distribution for the surfactant–ONu complexes at different N/P ratios for **S1** (left) and **S2** (right); 25 °C.

The analysis of the literature[31–33] on the ONu interactions with single-chained cationic surfactants revealed that the ONu-induced vesicle formation occurs in mixed systems, which was explored by scattering techniques, turbidimetry and fluorescence spectroscopy. Structural transitions were assumed to occur with an increase in surfactant concentration resulting in more compact ONu packing.[31–33] With this in mind we analyzed the size distribution in the ONu–surfactant systems (Fig. 7). Differences in the structural behavior of surfactants **S1** and **S2** have been revealed: (i) while **S1** tends to form large aggregates in both single and mixed solutions, their formation in the case of **S2** is induced by oligonucleotide; (ii) an increase in the **S1** concentration within the N/P ratio <1 only slightly affects the size distribution, with D_H of 150–200 nm prevailing; (iii) as the N/P ratio for **S1** approaches 1, the bimodal size distribution appears with the contribution of population in the submicron diapason. The N/P = 1 corresponds to the precipitation region whereupon the aggregates of 150 nm are returned; (iv) for the **S2**–ONu system, a sharp increase in the size occurs with the ONu addition; (v) before N/P = 1, the prevailing size of 150 to 200 nm is observed, with a short precipitation range occurring beyond the equimolar ratio; (vi) a decrease in D_H to $\leq$10 nm takes place at the higher surfactant concentration. Probably, the latter indicates that the saturation is attained at a definite surfactant/ONu ratio, whereupon free micelles appear in the solution. Such a behavior resembles the structural transitions in the surfactant–synthetic polymer systems.[11] Data on the zeta potential (Fig. 8) provide evidence for the charge compensation that begins from the N/P ratio of *ca.* 0.8 to 0.9, while complete recharging, *i.e.*, the attainment of the positive zeta potential occurs at N/P = 2.5 for **S1** and 3.0 for **S2**. These data are in agreement with the N/P critical ratio obtained by the EB exclusion study. Fluorescence emission spectra for the systems studied are shown in Fig. 9. These data were used to calculate the fraction of the oligonucleotide bound with a surfactant using the following expression: $\beta = (I_b - I_{obs})/(I_b - I_f)$, where I_f and I_b are the intensity of fluorescence of free EB and that bound with ONu, while I_{obs} is the observed intensity in titration measurements. The results of calculations (Fig. 10) show that the effective surfactant–ONu binding occurs within the component ratio from 0.8 to 2. A sharper increase in the β value is observed with an increase of the N/P ratio as compared to the zeta potential growth.

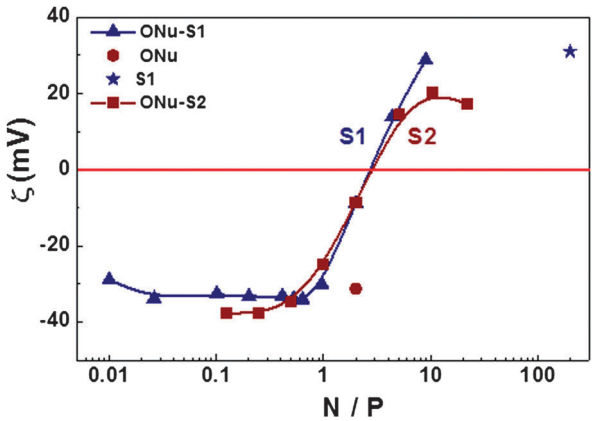

Fig. 8 Zeta potential of **S1**–ONu and **S2**–ONu complexes as a function of the N/P ratio, 25 °C.

Indeed, the ζ *versus* N/P plot tends to reach a plateau at the N/P ratio beyond 10 (Fig. 8), while a marked saturation of the binding degree β occurs at the lower component ratio close to 2 in the EB exclusion study (Fig. 10). Probably, this can be explained by the fact that charge compensation is mainly contributed by electrostatic interactions, while the surfactant–ONu complexation as a whole is mediated by the wider spectrum of intermolecular interactions, including H-bonding, hydrophobic effect, *etc.*

Interaction of the surfactants with the DPPC bilayer

In water, DPPC forms liposomes made up of closed bilayers, which can exist either in gel or liquid crystalline phases, depending on the temperature. For pure DPPC, the temperature of the transition between these phases, the so-called main phase transition or melting point (T_m), is *ca.* 41 °C,[34,35] while the introduction of surfactants may change this value. Different spectral methods were successfully used to study the behavior of pure phospholipid (PL) membranes and their perturbation by external reagents. According to ref. 35, "the assessment of membrane integrity as a change in suspension turbidity is perhaps the best known example of a spectroscopic method as applied to the study of membrane–surfactant interactions". Thermotropic phase transition has been monitored by turbidimetry in both natural and model membrane dispersions.[36,37]

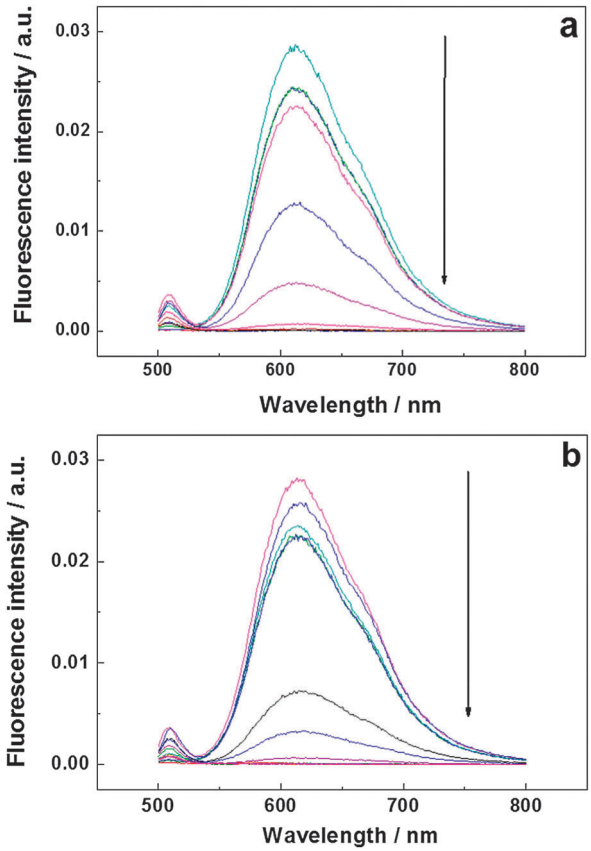

Fig. 9 Quenching of fluorescence of ethidium bromide in the presence of surfactant **S1** (a) and **S2** (b) at different surfactant–ONu molar ratios, 25 °C (the increment of the surfactant concentration is indicated by the arrow head).

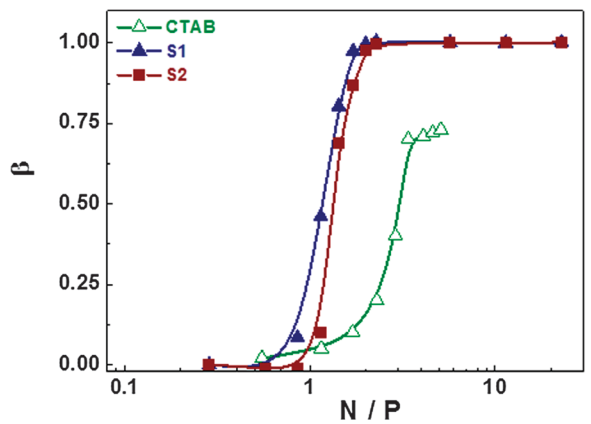

Fig. 10 Binding degree of oligonucleotide by cationic surfactants as a function of the N/P ratio calculated from the ethidium bromide exclusion data, 25 °C.

Fig. 11 shows the dependence of T_m on the surfactant/DPPC molar ratio (primary data are given in Fig. S5 and S6 in ESI†). A marked difference is observed in the interactions of **S1** and **S2** with the liposomes. In the presence of **S2**, a slight if any increase in T_m occurs indicating the stabilization of the gel-like ordering of the bilayer. At the same time, such a slight effect probably explains the very poor affinity of **S2** toward the membrane.

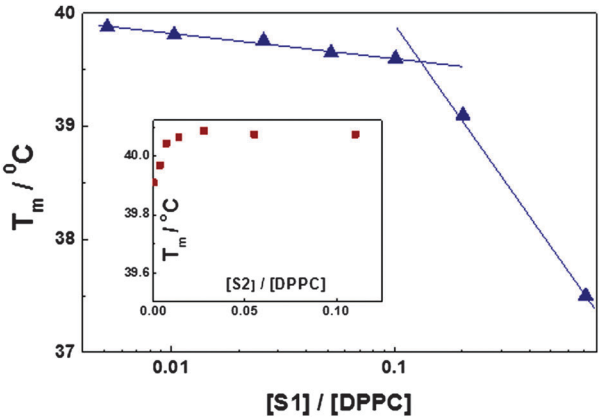

Fig. 11 Temperature of the main phase transition derived from turbidimetry titration data for DPPC liposomes as a function of surfactant/DPPC molar ratio for **S1** and **S2** (the inset); 0.7 mM DPPC; tris-HCl buffer; 25 °C.

The addition of the surfactant **S1** results in a decrease in the temperature of the main phase transition, which is probably due to the weakening of the chain interactions in the bilayer. A gradual decrease is observed before the breakpoint around the **S1**/DPPC ratio 0.14, which probably corresponds to the saturation of PL bilayers with surfactant molecules and to the onset of the solubilization of liposomes. The low 1 : 7 threshold ratio may result from the presence of a bulky diterpenoid moiety playing the role of hydrophobic fragments in the molecule of **S1**. Probably their effect resembles that of cholesterol, which can disturb lipid bilayers thereby increasing their fluidity and changing the interface curvature (Scheme 1).

In recent years, cationic liposomes have drawn increased attention, and many new cationic lipids have been synthesized to enhance the efficiency of gene and drug delivery.[38] However, modification of zwitter-ionic liposomes with cationic surfactants could be an easier and cheaper way to achieve the aim. Therefore, synthetic cationic surfactants were often used as helper additives to play a role in improving the properties, such as fluidity, permeability, curvature, surface potentials, and so on.[39] Therefore, the revealed ability of surfactant **S1** to integrate with the lipid bilayer provides evidence that **S1** may be used as a helper

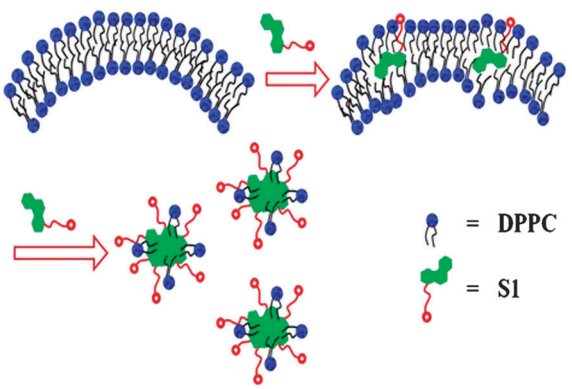

Scheme 1 The surfactant disordering effect on the lipid bilayer.

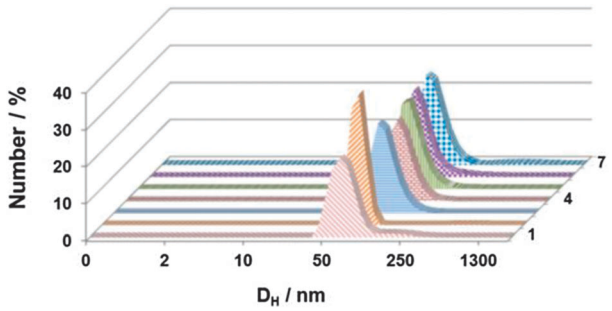

Fig. 12 Number averaged size distribution for **S1**–DPPC mixed aggregates as a function of surfactant/DPPC molar ratio; 0.7 mM single DPPC (1); DPPC/**S1** = 25 (2); 17 (3); 15 (4); 13 (5); 11 (6); 7 (7); 25 °C.

surfactant for the design of smart nanocontainers bearing a positive surface charge.

To test this assumption we have investigated the **S1**–DPPC aggregates, focusing on the following points. First, the size and zeta potential were estimated to demonstrate the nanoscale dimension of the system and the appearance of the positive charge on the aggregate surfaces. Second, the binding capacities of single and mixed systems toward the water-insoluble probe have been investigated. As can be seen in Fig. 12, *ca.* 70–90 nm aggregates are formed at the low surfactant fraction, while *ca.* 150 nm assemblies occur near the critical **S1**/DPPC ratio of 0.14. Importantly, the transition occurs from the near-zero zeta potential to the positive values of *ca.* +10 mV (Fig. S7, ESI†).

The dye solubilization study revealed that the single surfactant solution demonstrates a high solubilization capacity toward hydrophobic probe Sudan I (Fig. S8, ESI†). We studied only the concentration range above the critical point of 0.025 M, where micelle-like aggregates probably occur. The linear dependence has been observed, with the slope characterizing the solubilization power (S) of aggregates toward Sudan I. This value is determined by the number of moles of solubilized dyes per moles of aggregated surfactants. It can be calculated as follows: $S = b/\varepsilon$, where b is the slope of the A *versus* C plot (Fig. 13), and ε is the extinction coefficient of the dye

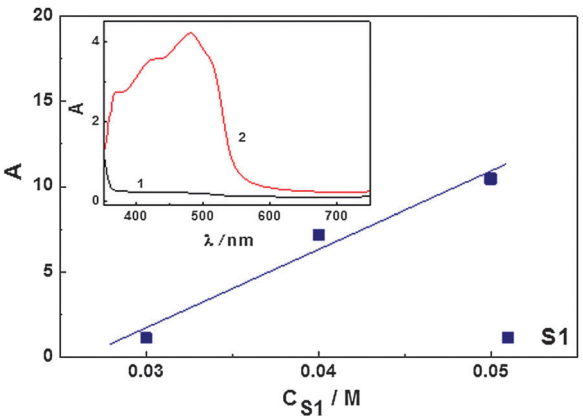

Fig. 13 Absorbency of Sudan I at 500 nm in single **S1** solution as a function of surfactant concentration. In the inset: visible spectrum of Sudan I in the single liposome (1) and mixed **S1**–DPPC system (2); 25 °C.

(8700 L mol^{-1} cm^{-1}). Values of b = 467.5 and S = 0.054 are obtained for surfactant **S1**. Importantly, unlike the pure DPPC system, mixed **S1**–DPPC aggregates demonstrate a rather high solubilization capacity (Fig. 13, inset). This finding may be successively used for control the binding/release behavior by varying the **S1**/DPPC ratio.

The effect of the surfactant S1 on the DNA transfer

The ability of surfactants studied to interact with oligonucleotide and to integrate with the lipid bilayer demonstrate their potentiality in biotechnologies aimed at gene delivery. Therefore, the DNA transfer into prokaryotic cells is studied herein. Unlike mammalian cells, the integrity of the bacterium cells is preserved by the cell wall, which protects bacteria from osmotic lysis. The transformation protocols with bacteria were developed much earlier than those for the gene transfection into mammalian cells.[40,41] Nevertheless many problems associated with gene delivery are better studied for the latter. Thus, amphiphilic carriers especially those with cationic fragments are widely used as DNA carriers to eukaryotic systems,[7,8] while few works are available on bacterium transformation with the help of the DNA–surfactant complexes.[20]

There are different methods that are used to introduce plasmid DNA into cells, including chemical treatment[42] and physical protocols, such as electroporation, ultrasound or microwave impact,[43,44] *etc.* The survey of literature[45–47] motivates us to study the surfactants as potential excipients for gene delivery formulations in both chemical and direct physical protocols, *i.e.* electroporation. Among the probable mechanism of the surfactant function upon electroporation, the following effects may be assumed: (i) changes of the electroporation threshold due to the chemical modification of a lipid bilayer; (ii) an increase in the plasmid uptake due to the surfactant involvement into the DNA complexation; (iii) the reduced tissue damage due to re-sealing the electropermeabilized cells. Different types of surfactants are shown to exert various effects. For a nonionic surfactant and block copolymer, both an increase and decrease in the electroporation threshold are documented depending on their structure and concentration.[48–50] According to ref. 20, there are effective formulations based on cationic amphiphiles that promote the transfer of DNA into bacteria. An enhanced efficiency of transformation was observed in the presence of cationic lipids at the 1 : 0.5 N/P ratio, whereas a decrease in the number of transformed cells occurs with an excess of amphiphiles.[20]

Taking into account the above information, the influence of **S1** on the DNA transfer through electroporation technique has been estimated. The cell cultures of *E. coli* Nova Blue were transformed by complexes pDNA–**S1** at different N/P ratios (Table S1, ESI†). According to the results given in Fig. 14, the efficiency of transformation decreases with an increase in the N/P ratio. It should be noted that in some cases the potential therapeutic applications from the transformation inhibition effect of **S1** and **S2** may be needed.[51] For example, definite diseases are provoked by the excess gene function noncharacteristic for a normal cell. In this case gene therapy has to be

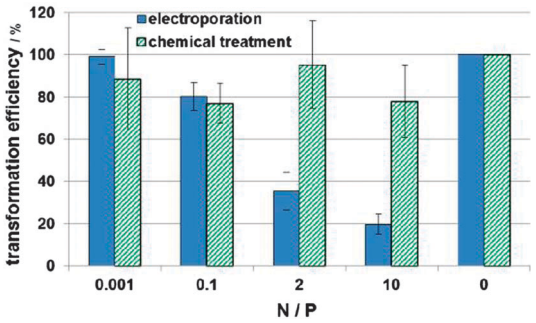

Fig. 14 Effect of the **S1** concentration on transformation efficiency for different protocols used: electroporation (filled) and chemical treatment (shaded).

directed onto the suppression of superactive gene by means of constructions which would express into the cells factors capable of interacting with an expression product of an unwanted gene, thereby neutralizing its harmful effect.

Another protocol involved the chemical treatment of bacteria with $CaCl_2$, which induces the permeability of the cell walls (Table S2, ESI†). In this case, no significant effect on the number of cells transformed has been revealed (Fig. 14). To explain these results, different transformation events should be analyzed, *i.e.* (i) the DNA complexation by the surfactant; (ii) the uptake of DNA across the membrane, and (iii) its establishment in the cell interior.

Fig. 15 shows images of the agarose gel electrophoresis of the surfactant–DNA complexes of different charge ratios. Surprisingly, the migration of plasmid DNA in the gel is practically uninfluenced by surfactants. This result would make it clear why there is no positive effect of the surfactant on the cell transformation. However it gives no explanation of the inhibition mentioned above.

The negative effect of surfactant **S1** could be accounted for the fact that cationic surfactants probably exhibit antibacterial activity. Indeed, cationic amphiphiles can interact with bacterial cell membranes bearing a high negative charge and disrupt

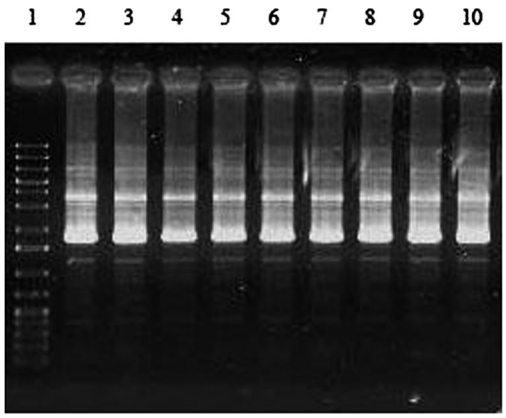

Fig. 15 Images of the agarose gels electrophoresis of the surfactant–DNA complexes of different charge ratios; GeneRuler 1331 (Fermentas) (1); single pK18 (6); pK18 + **S2** at N/P = 0.002 (2); 0.02 (3); 4 (4); 22 (5); pK18 + **S1** at N/P = 0.002 (7); 0.02 (8); 4 (9); 22 (10).

their integrity, which exerts a fatal effect on bacteria.[52] Therefore the inhibition activities of **S1** and **S2** toward microbes are tested. No antibacterial activity has been revealed (Table S3, ESI†), which suggests that the decrease of the number of transformed bacteria is not associated with the toxicity of the surfactants. This result, along with the data on the preservation of the transformation efficacy in the case of chemically-induced cell permeability, provide evidence that (i) the integrity of cell membranes is not disrupted by **S1**, and (ii) the pDNA–**S1** complexes are viable within the cell interior. It should be concluded that the negative effect of surfactant **S1** on the electroporation procedure is responsible for the decrease in the transformation efficacy. It has been documented[53] that the intracellular uptake of small molecules using the electroporation protocol occurs through the diffusion at poles facing both positive (the larger area of permeabilized membrane) and negative (the larger degree of permeabilization) electrodes. The DNA uptake occurs through the pole facing the negative electrode and is facilitated by the field carrying the polynucleotide macroanion towards the anode. The involvement of the cationic surfactant may result in weakening the electrophoretic effect of the field due to the compensation of the cathode potential or charge density of phosphate anions.

Conclusion

The self-assembly of the newly synthesized diterpenoid surfactants with ammonium head groups and bromide (**S1**) or tosylate (**S2**) counterions has been studied, and characteristics of aggregates significant for the current biotechnological strategies, *i.e.* cmc and size have been estimated. Although their cmcs differ inconsiderably, the structural behavior is strongly dependent on the counterion structure. Compound **S2** forms micelles in the whole concentration range, while in the **S1** aqueous solution large aggregates with hydrodynamic diameter of *ca.* 150 nm are formed in the concentration range before the second threshold near ~0.025–0.03 M. Beyond this point, small micelles exist with a D_H of *ca.* 5 nm. The difference in organic *versus* inorganic counterions is typically treated in terms of higher affinity of the former toward the aggregate surface,[54–57] which in turn may have an impact on their functional activity.[56,57] Based on this trend, a lower cmc and closer packing mode may be predicted for **S2** as compared to **S1**. However, very similar cmc values observed for diterpenoid surfactants indicate that other factors rather than counterion binding control the structural behavior of these amphiphiles. Larger size and higher aggregation numbers obtained for **S1** aggregates between the cmc and a second critical concentration assume a closer packing of the **S1** molecules. Probably the location of bulky tosylate-ions between head groups may prevent the close packing the surfactant molecules and distance them from each other, thus increasing the surface curvature and provoking the formation of micelle-like aggregates. The difference in the morphological behavior is probably responsible for their different effects on the interaction with a lipid bilayer. Unlike the **S2** compound, **S1** can integrate with

liposomes based on dipalmitoylphosphatidylcholine, resulting in a decrease of the temperature of the main phase transition. This may be due to the similarity in the association model of **S1** and liposomes (the closed bilayer) accounting for their compatibility. Another factor is the counterion effect on the water structure, which in its turn can influence the hydrophobic effect controlling the aggregation behavior. The role of the counterion nature on the lipid thermotropic properties and vesicle-to-micellar transition is elucidated in the literature for the Br–Cl pair,[58,59] and is ever more pronounced for the Br–Tos pair. Both surfactants, **S1** and **S2**, demonstrate an effective complexation capacity toward oligonucleotide, which is supported by recharging the surfactant–ONu complexes and the ethidium bromide exclusion at the low N/P ratio. Meanwhile, the low complexation of plasmid DNA with the surfactants has been revealed in the gel electrophoresis experiments. The DNA transfer to bacterium cells mediated by the surfactant **S1** has been shown to depend on the protocol used. In the case of the electroporation, the inhibition of the cell transformation occurs in the presence of the surfactants, while upon the chemical treatment, no surfactant effect has been observed. The data obtained have revealed that (i) even minor changes in the molecular structure of amphiphiles beyond their chemical nature may dramatically affect their solution behavior; and (ii) the compounds studied may be ranked as a single carrier or as a helper surfactant for the design of the positively charged nanocontainers.

Acknowledgements

We thank the Russian Foundation for Basic Researches (grants no. 13-03-97075, 12-03-01085) and the Russian Academy of Sciences for financial support.

References

1 M. Ramanathan, L. K. Shrestha, T. Mori, Q. Ji, J. P. Hill and K. Ariga, *Phys. Chem. Chem. Phys.*, 2013, **15**, 10580–10611.
2 P. Angelikopoulos and H. Bock, *Phys. Chem. Chem. Phys.*, 2012, **14**, 9546–9557.
3 E. M. Shchukina and D. G. Shchukin, *Adv. Drug Delivery Rev.*, 2011, **63**, 837–846.
4 K. Ariga, Yu. M. Lvov, K. Kawakami, Q. Ji and J. P. Hill, *Adv. Drug Delivery Rev.*, 2011, **63**(9), 762–771.
5 A. Sprunk, C. J. Strachan and A. Graf, *Eur. J. Pharm. Sci.*, 2012, **46**(5), 508–515.
6 V. P. Torchilin, *Adv. Drug Delivery Rev.*, 2012, **64**, 302–315.
7 R. Dias, S. Mel'nikov, B. Lindman and M. G. Miguel, *Langmuir*, 2000, **16**(24), 9577–9583.
8 A. Dasgupta, P. K. Das, R. S. Dias, M. G. Miguel, B. Lindman, V. M. Jadhav, M. Gnanamani and S. Maiti, *J. Phys. Chem. B*, 2007, **111**(29), 8502–8508.
9 E. Mosettig and W. R. Nes, *J. Org. Chem.*, 1955, **20**(7), 884–899.
10 S. Madan, S. Ahmad, G. N. Singh, K. Kohli, Y. Kumar, R. Singh and M. Garg, *Indian J. Nat. Prod. Resour.*, 2010, **1**(3), 267–286.
11 K. Holmberg, B. Jönsson, B. Kronberg and B. Lindman, *Surfactants and Polymers in Aqueous Solution*, John Wiley & Sons, Ltd, Chichester, 2007.
12 H. Fendler, *Membrane Mimetic Chemistry: Characterizations and Applications of Micelles, Microemulsions, Monolayers, Bilayers, Vesicles, Host-Guest Systems, and Polyions*, Wiley-Interscience, New York, 1982.
13 N. B. Bowden, M. Weck, I. S. Choi and G. M. Whitesides, *Acc. Chem. Res.*, 2001, **34**, 231–238.
14 R. N. Khaibullin, I. Yu. Strobykina, V. E. Kataev, O. A. Lodochnikova, A. T. Gubaidullin and R. Z. Musin, *Russ. J. Gen. Chem.*, 2009, **79**(5), 967–971.
15 M. A. Hayat and S. E. Miller, *Negative Staining*, McGraw-Hill Publishing, New York, 1990.
16 D. A. Faizullin, N. N. Vylegzhanina, O. I. Gnezdilov, V. V. Salnikov, A. V. Galukhin, I. I. Stoikov, I. S. Antipin and Y. F. Zuev, *Appl. Magn. Reson.*, 2011, **40**, 231–243.
17 N. J. Turro and A. Yekta, *J. Am. Chem. Soc.*, 1978, **100**, 5951–5952.
18 K. Kalyanasundaran and J. K. Thomas, *J. Am. Chem. Soc.*, 1977, **99**, 2039–2044.
19 R. Anthony, *Transformation of Competent Bacterial Cells: Electroporation*, John Wiley & Sons, Ltd, London, 2003.
20 D. Demir, F. Oner and T. Kocagoz, *FABAD J. Pharm. Sci.*, 2004, **29**, 7–13.
21 L. Ya. Zakharova, V. V. Syakaev, M. A. Voronin, V. E. Semenov, F. G. Valeeva, A. R. Ibragimova, A. V. Bilalov, R. Kh. Giniyatullin, S. K. Latypov, V. S. Reznik and A. I. Konovalov, *J. Colloid Interface Sci.*, 2010, **342**, 119–127.
22 M. A. Voronin, D. R. Gabdrakhmanov, R. N. Khaibullin, I. Yu. Strobykina, V. E. Kataev, B. Z. Idiyatullin, D. A. Faizullin, Y. F. Zuev, L. Ya. Zakharova and A. I. Konovalov, *J. Colloid Interface Sci.*, 2013, **405**, 125–133.
23 J. Aguiar, P. Carpena, J. A. Molina-Bolívar and C. Carnero Ruiz, *J. Colloid Interface Sci.*, 2003, **258**, 116–122.
24 N. J. Turro and P.-L. Kuo, *J. Phys. Chem.*, 1986, **90**, 4205–4210.
25 Ch. Honda, M. Itagaki, R. Takeda and K. Endo, *Langmuir*, 2002, **18**, 1999–2003.
26 T. Morisue, Y. Moroi and O. Shibata, *J. Phys. Chem.*, 1994, **98**, 12995–13000.
27 O. Zheng and J.-X. Zhao, *J. Colloid Interface Sci.*, 2006, **300**, 749–754.
28 Kabir-ud-Din, M. Shafi, P. A. Bhat and A. A. Dar, *J. Hazard. Mater.*, 2009, **167**, 575–581.
29 I. V. Grigoriev, V. A. Korobeynikov, S. V. Cheresiz, A. G. Pokrovskiy, L. Ya. Zakharova, M. A. Voronin, S. S. Lukashenko, A. I. Konovalov and Y. F. Zuev, *Dokl. Biochem. Biophys.*, 2012, **445**(1), 197–199.
30 L. Zakharova, M. Voronin, D. Gabdrakhmanov, V. Semenov, R. Giniyatullin, V. Syakaev, S. Latypov, V. Reznik, A. Konovalov and Y. Zuev, *ChemPhysChem*, 2012, **13**, 788–796.
31 X. Guo, H. Li, F. Zhang, S. Zheng and R. Guo, *J. Colloid Interface Sci.*, 2008, **324**, 185–191.
32 X. Liu and N. L. Abbott, *J. Phys. Chem. B*, 2010, **114**, 15554–15564.
33 D. Santhiya, R. S. Dias, A. Shome, P. K. Das, M. G. Miguel, B. Lindman and S. Mait, *Langmuir*, 2009, **25**, 13770–13775.

34 R. Koynova and M. Caffrey, *Biochim. Biophys. Acta, Rev. Biomembr.*, 1998, **1376**, 91–145.
35 F. M. Goñi and A. Alonso, *Biochim. Biophys. Acta, Biomembr.*, 2000, **1508**, 51–68.
36 M. B. Abramson, *Biochim. Biophys. Acta, Biomembr.*, 1971, **225**, 167–170.
37 J. A. S. Almeida, S. P. R. Pinto, Y. Wang, E. F. Marques and A. A. C. C. Pais, *Phys. Chem. Chem. Phys.*, 2011, **13**, 13772–13782.
38 V. Gopal, T. K. Prasad, N. M. Rao, M. Takafuji, M. M. Rahman and H. Ihara, *Bioconjugate Chem.*, 2006, **17**(6), 1530–1536.
39 C. N. C. Sobral, M. A. Soto and A. M. Carmona-Ribeiro, *Chem. Phys. Lipids*, 2008, **152**, 38–45.
40 S. D. Cosloy and M. Oishi, *Proc. Natl. Acad. Sci. U. S. A.*, 1973, **70**, 84–87.
41 S. N. Cohen, A. C. Y. Chang and L. Hsu, *Proc. Natl. Acad. Sci. U. S. A.*, 1972, **69**, 2110–2114.
42 M. Mandel and A. Higa, *Biotechnology*, 1992, **24**, 198–201.
43 L. Drury, *Methods Mol. Biol.*, 1994, **31**, 1–8.
44 R. Fregel, V. Rodriguez and V. M. Cabrera, *Lett. Appl. Microbiol.*, 2008, **46**, 498–499.
45 R. Draghia-Akli, A. S. Khan, M. A. Pope and P. A. Brown, *Gene Ther. Mol. Biol.*, 2005, **9**, 329–338.
46 R. C. Lee, L. P. River, F. S. Pan, L. Ji and R. L. Wollmann, *Proc. Natl. Acad. Sci. U. S. A.*, 1992, **89**, 4524–4528.
47 S. N. Murthy, A. Sen and S. W. Hui, *J. Controlled Release*, 2004, **98**, 307–315.
48 G. C. Troiano, L. Tung, V. Sharma and K. J. Stebe, *Biophys. J.*, 1998, **75**, 880–888.
49 V. Sharma, K. Stebe, J. C. Murphy and L. Tung, *Biophys. J.*, 1996, **71**, 3229–3241.
50 Ju. Hartikka, L. Sukhu, C. Buchner, D. Hazard, V. Bozoukova, M. Margalith, W. K. Nishioka, C. J. Wheeler, M. Manthorpe and M. Sawdey, *Mol. Ther.*, 2001, **4**, 407–415.
51 K. Kawabata, K. Tashiro, F. Sakurai, N. Osada, J. Kusuda, T. Hayakawa, K. Yamanishi and H. Mizuguchi, *Gene Ther.*, 2007, **14**, 1199–1207.
52 J. A. Castillo, A. Pinazo, J. Carilla, M. R. Infante, M. A. Alsina, I. Haro and P. Clapes, *Langmuir*, 2004, **20**, 3379–3387.
53 J. Gehl, *Acta Physiol. Scand.*, 2003, **177**, 437–447.
54 S. Manet, Y. Karpichev, D. Bassani, R. Kiagus-Ahmad and R. Oda, *Langmuir*, 2010, **26**(13), 10645–10656.
55 E. Feitosa, M. R. S. Brazolin, R. M. Z. G. Naal, M. P. Freire de Morais Del Lama, J. R. Lopes, W. Loh and M. Vasilescu, *J. Colloid Interface Sci.*, 2006, **299**, 883–889.
56 L. Ya. Zakharova, L. A. Kudryavtseva and A. I. Konovalov, *Mendeleev Commun.*, 1998, **8**(4), 163–164.
57 L. Ya. Zakharova, S. B. Fedorov, L. A. Kudryavtseva, V. E. Bel'skii and B. E. Ivanov, *Russ. Chem. Bull.*, 1993, **42**(8), 1329–1333.
58 E. Feitosa and F. R. Alves, *Chem. Phys. Lipids*, 2008, **156**, 13–16.
59 E. Feitosa, N. M. Bonassi and W. Loh, *Langmuir*, 2006, **22**, 4512–4517.